Cell Dynamics Simulations of Microphase Separation in Block Copolymers

S. R. Ren and I. W. Hamley*

School of Chemistry, University of Leeds, Leeds LS2 9JT, UK

Received April 19, 2000; Revised Manuscript Received October 10, 2000

ABSTRACT: Cell dynamics simulations of ordered structures formed in diblock copolymer melts were performed to investigate the effects of simulation parameters on the morphological features and kinetics of ordering from the initial disordered state. We show that sphere, cylinder, lamellar, and bicontinuous structures can all be simulated with an appropriate choice of system parameters. The simulation parameters are related to the expansion parameters in the Landau free energy in the Cahn−Hilliard−Cook equation, of which the cell dynamics equations are a coarse-grained discretization. The extent of segregation is found to increase as the effective diffusion coefficient decreases. It is shown that the magnitude of the long-range repulsive contribution to the free energy has to be defined within certain limits to produce morphologies that resemble those observed experimentally. The formation of ordered structures is found to be quicker, as expected, for deeper quenches, which also produce more strongly segregated structures. Addition of random thermal noise proves to be essential to generate spherical structures, formed in the high-temperature ordered phase region. Thermal noise also acts to increase the ordering kinetics.

Introduction

Block copolymers are a fascinating class of soft material that can self-assemble into nanoscale ordered structures due to microphase separation. For diblock copolymers, lamellar (lam), hexagonal-packed cylinder (hex), bicontinuous cubic gyroid (gyr), and body-centered cubic (bcc) structures have all been confirmed as equilibrium structures.[1] Self-consistent-field theory for the thermodynamics of block copolymers[2−4] is one of the most successful models in soft condensed matter physics, providing semiquantitative predictions for phase boundaries as well as domain spacings and interface widths among other structural characteristics. However, this method is computationally demanding, and there is a need for efficient methods to model dynamic processes at the mesoscale level such as ordering kinetics, defect dynamics, dynamics of shear-induced orientation, etc. The cell dynamics simulation (CDS) method is a very promising approach to modeling such phenomena.

The cell dynamics simulation method is an example of a cellular automaton, developed to model interface dynamics in phase-separating systems.[5−7] The time evolution of an order parameter is evaluated on a lattice, according to two mechanisms. The first arises from the local driving force due to chemical potential gradients. The second allows for the connectivity of the cells and corresponds to diffusive dynamics due to order parameter variations in neighboring cells.

Cell dynamics simulations have been extensively used to simulate spinodal decomposition in binary blends[5−10] and also the effect of shear on this process.[11,12] This powerful method has also found broad applications in simulating phase separation dynamics in other systems with competing short- and long-range interactions. Examples include microemulsions,[13,14] binary blends containing surfactants[15] or hard particles,[16] granular materials,[17] polymer-dispersed liquid crystals,[18] and cross-linked polymer blends.[19] However, in this paper the focus is on the application of the CDS method to simulate microphase-separated structures in block copolymers and the kinetics of microphase separation.

Although the CDS equations model interfacial dynamics independent of any free energy, it has been shown that the scheme corresponds to a coarse-grained discretization of the time-dependent Ginzburg−Landau (TDGL) equation for a system with a nonconserved order parameter or the Cahn−Hilliard−Cook (CHC) equation for phase separation in which the order parameter is conserved.[6] Block copolymer microphase separation belongs to the latter class of phase transition, although the dynamics do not belong to the CHC universality class due to the existence of a long-range interaction. The coarse-graining that is inherent in the CDS equations is the source of its advantages compared to molecular simulation techniques, since the CHC (or TDGL) equation is modeled on mesoscopic length scales and long time scales where details of molecular motions can be neglected.

The first cell dynamics simulations for block copolymers were of two-dimensional stripe patterns.[20] The effect of thermal noise on domain coarsening in these structures has been studied.[21,22] The kinetics of growth of the stripe pattern have also been modeled in the zero noise limit.[23] Other investigators have examined the effect of shear on two-dimensional stripe[13] and hexagonal patterns,[24] and the effects of directional quenching (moving thermal boundary) has also been simulated.[25] However, less attention has been devoted to cell dynamics simulations of three-dimensional structures focusing on the effects of thermal noise (and other parameters in the model), nor on the effect of the kinetics of ordering of these structures from the disordered phase. Cell dynamics simulations of three-dimensional block copolymer morphologies have been performed by Qi and Wang,[26,27] who focused on the kinetics of order−order phase transitions, starting from initially oriented lamellar, hexagonal, and body-centered-cubic phases. Previ-

* Author for correspondence.

10.1021/ma000678z CCC: $20.00
Published on Web 12/08/2000

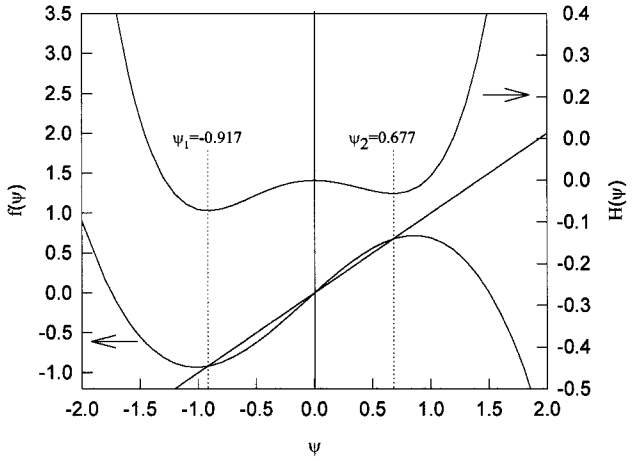

Figure 1. Free energy function $H(\psi)$ (top) and map function $f(\psi)$ (bottom) obtained for the parameters $A = 1.5$, $\tau = 0.32$, $f = 0.46$, $u = 0.5$, and $v = 1.5$. This corresponds to an ordered cylinder phase.

ous CDS studies of block copolymers have been reviewed.[28]

The dynamic mean-field density functional model introduced by Fraaije and co-workers has also been used to simulate three-dimensional structures in block copolymer melts[29,30] and solutions.[31] This model uses similar kinetic equations to the cell dynamics approach, but with an empirical mapping of the coefficients onto correlation functions obtained from bead models for Gaussian chains.[32]

In addition to demonstrating that the cell dynamics method is able to generate a range of observed melt morphologies for diblock copolymer melts, we systematically investigate the effects of the simulation parameters on the final morphology. These include the effective diffusion constant, the long-range interaction term, and thermal noise. Finally, the kinetics of ordering from the disordered initial configuration are investigated.

Cell Dynamics Method

In the cell dynamics method, an appropriate order parameter is discretized on a lattice, taking values $\psi(t,i)$ in cell i at time t. For diblock copolymers, a suitable choice is the compositional order parameter

$$\psi(\mathbf{r}) = \phi_A(\mathbf{r}) - \phi_B(\mathbf{r}) + (1 - 2f) \tag{1}$$

where ϕ_A and ϕ_B are local volume fractions of blocks A and B and f is the fraction of A monomers in the diblock. The evolution of the order parameter in an individual cell is represented by an equation of the form

$$\psi(t+1,i) = f(\psi(t,i)) \tag{2}$$

where $f(\psi)$ represents the so-called map function.[6] This function mimics the tendency of the order parameter to approach a nonzero value below the order−disorder transition. As sketched in Figure 1, for a phase transition described by a Landau free energy containing terms up to ψ^4, the function $f(\psi)$ needs to possess one hyperbolic source at the origin (corresponding to the high-temperature $\langle\psi\rangle = 0$ state) and two hyperbolic sinks, corresponding to the ordered state, in which the order parameter takes either of the two values $\langle\psi\rangle = \psi_1, \psi_2$. Although Figure 1 indicates how a suitable form for $f(\psi)$ can be deduced from a ψ^4 free energy functional, the free energy functional itself is not required to construct a CDS model.[6] Spatially cooperative dynamics are included in cell dynamics simulations via a diffusive mechanism due to the connectivity of cells. For the case of a nonconserved order parameter, the time evolution of the order parameter is represented by[6] by the sum of a term related to chemical potential gradients and a term that accounts for diffusive dynamics:

$$\psi(t+1,i) = f(\psi(t,i)) + D[\langle\langle\psi(t,i)\rangle\rangle - \psi(t,i)] = \Gamma[\psi(t,i)] \tag{3}$$

In eq 3, D is a positive constant that plays the role of a diffusion coefficient, and $\langle\langle X\rangle\rangle - X$ is essentially the isotropized discrete Laplacian. For a three-dimensional cubic lattice, the form

$$\langle\langle\psi(r,t)\rangle\rangle = \frac{6}{80}\sum_{i\in\{NN\}}\psi(\mathbf{r}_i,t) + \frac{3}{80}\sum_{i\in\{NNN\}}\psi(\mathbf{r}_i,t) + \frac{1}{80}\sum_{i\in\{NNNN\}}\psi(\mathbf{r}_i,t) \tag{4}$$

has been reported[10] to be satisfactorily isotropic, although it may not be the optimal choice (here NN denotes nearest neighbor, NNN next-nearest neighbor, etc.).

For a conserved order parameter, there should be no net change of order parameter in the region surrounding a given cell. Since the net gain of order parameter in a particular cell is given by $\Gamma[\psi(t,n)] - \psi(t,n)$, the CDS model for a conserved order parameter becomes[6]

$$\psi(t+1,i) = \Gamma[\psi(t,i)] - \langle\langle\Gamma[\psi(t,i)] - \psi(t,i)\rangle\rangle \tag{5}$$

For block copolymers, the long-range ordering of the microstructure leads to an additional term, $-B\psi(t,i)$.[20] This term arises from the contribution of long-range ordering to the free energy,[33] as discussed below. In addition, a thermal noise term is introduced to allow for compositional fluctuations. This is represented as $\eta\xi(t,i)$ where η is the amplitude of the noise $\xi(t,i)$, taken from a Gaussian random noise distribution.[34] Thus, the cell dynamics equation used herein is

$$\psi(t+1,i) = \Gamma[\psi(t,i)] - \langle\langle\Gamma[\psi(t,i)] - \psi(t,i)\rangle\rangle - B\psi(t,i) + \eta\xi(t,i) \tag{6}$$

The cell dynamics equations can be shown to correspond to a coarse-grained discretization of the Cahn−Hilliard−Cook equation[6]

$$\frac{\partial\psi}{\partial t} = M\nabla^2\left(\frac{\delta F(\psi)}{\delta\psi}\right) + \eta\xi(\mathbf{r},t) \tag{7}$$

where M is a phenomenological mobility constant ($M = 1$ is assumed) and $F(\psi)$ is the free energy functional, consisting of short-range and long-range interaction terms,

$$F(\psi) = F_S(\psi) + F_L(\psi) \tag{8}$$

The short-range interaction term is written as

$$F_S(\psi) = \int d\mathbf{r}\left[H(\psi) + \frac{D}{2}(\nabla\psi(r))^2\right] \tag{9}$$

where $H(\psi)$ is a free energy function,

$$H(\psi) = \left[-\frac{\tau}{2} + \frac{A}{2}(1-2f)^2\right]\psi(r)^2 + \frac{v}{3}(1-2f)\psi(r)^3 + \frac{u}{4}\psi(r)^4 \quad (10)$$

Here τ is a temperature-like parameter and A, v, and u are phenomenological constants, while $f = N_A/(N_A + N_B)$ is the composition of the copolymer. The free energy functional has two minima in an ordered phase for sufficiently large and positive τ.

The long-range interaction term is given by[33]

$$F_L(\psi) = \frac{B}{2}\int d\mathbf{r} \int d\mathbf{r}'\, G(\mathbf{r}-\mathbf{r}')\,\psi(\mathbf{r})\,\psi(\mathbf{r}') \quad (11)$$

where the Green's function for the Laplace equation $\nabla^2 G(\mathbf{r}-\mathbf{r}') = -\delta(\mathbf{r}-\mathbf{r}')$. Making the approximations $\psi(\mathbf{r},t+1) - \psi(\mathbf{r},t) \approx \partial\psi/\partial t$ and $\nabla^2 X \approx \langle\langle X\rangle\rangle - X$ and subtracting $\psi(t,i+1)$ from both sides of eq 6, we find that

$$\frac{\partial\psi}{\partial t} = \nabla^2\psi - \nabla^2[f(\psi) + D\nabla^2\psi] - B\psi + \eta\xi \quad (12)$$

This can be compared to eq 7, leading to an identification of the map function

$$f(\psi) = [1 + \tau - A(1-2f)^2]\psi - v(1-2f)\psi^2 - u\psi^3 \quad (13)$$

We have chosen to use this polynomial form rather than the usual symmetric function $f(\psi) = A\tanh(\psi)$ used in cell dynamics simulations,[5,6] in order to allow in a straightforward manner for the asymmetric free energy functional when a cubic term is included in eq 10, as required to account for the formation of hexagonal and cubic phases when using a Landau free energy. A polynomial map function, similar to eq 13, although without a quadratic term, was derived from the cell dynamics equations for phase-separating systems using an isotropic two-dimensional Laplacian.[35] The linear term in eq 13 also has a prefactor that differs from that obtained by Teixeira and Mulder because we have chosen to write eq 10 in the form used by Qi and Wang.[27] Teixeira and Mulder[35] have also established relations between polynomial and hyperbolic tangent forms for the map.

Results and Discussion

Free Energy and Phase Diagram. Although the cell dynamics model does not rely on a particular free energy functional, it is necessary to specify a map function $f(\psi)$ such that $f(\psi) = \psi_1, \psi_2$ corresponding to the order parameter at two minima in an asymmetric double-well free energy. This is illustrated in Figure 1. The free energy form ($H(\psi)$) given by eq 10 possesses two minima in an ordered microphase, as illustrated in Figure 1 for an asymmetric block copolymer ($f = 0.46$). The map function $f(\psi)$ defined in eq 13 is also shown in the figure together with a straight line ($\psi = f(\psi)$) to indicate the microphase separation path.

The free energy corresponding to the cell dynamics equation is given by eq 8 and includes both short-range and long-range contributions. The free energy can be written analytically in the mean-field approximation for arbitrary degrees of segregation via self-consistent-field theory.[2,4] Expressions for the free energy in the limit of weak[36] and strong segregation[33,37] have also been obtained. However, all of these theories require that the symmetry of the phase be specified a priori in order to calculate the free energy. In contrast, cell dynamics simulations do not require the free energy to be specified, so that it is possible to simulate a range of structures without a priori assumptions on symmetry. The cell dynamics phase diagram is however complex, since B and D in eq 9 and eq 11 and the coefficients in the Landau free energy, eq 10, can all be varied. In this paper, we explore the effect of variation of B and D on the observed morphology, using the Landau free energy, eq 10, as a "road map". In other words, the Landau free energy is used as a guide to the morphology to be expected, although the final structure may differ depending on the value of B and D. The structures in the Landau mean-field phase diagram will be obtained in the limits $B = 0$, $D = 0$. Although the Landau phase diagram is only valid in the weak segregation limit, the cell dynamics simulations apply equally well to the strong segregation limit, because the free energy, eq 8, has the same form in the weak and strong segregation regime, provided that a suitably symmetric form of the local free energy is chosen.[33]

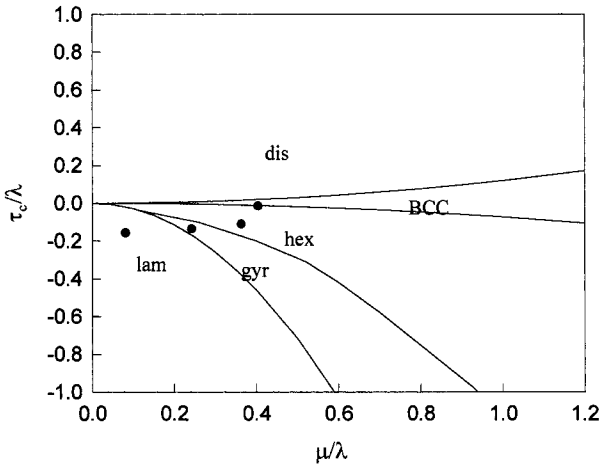

Figure 2. Landau mean-field phase diagram. In terms of the parameters in eq 10, $\lambda = 6u$, $\tau_c = -\tau + A(1-2f)^2$, and $\mu = 2v(1-2f)$. This change of variables gives the phase diagram presented by Podneks and Hamley,[42] following Marques and Cates[38] (who did not consider the bicontinuous structure). The points correspond to parameters for the simulations of different phases (see Figure 3).

The phase diagram derived from Landau mean-field theory is shown in Figure 2. The phase boundaries for disordered, body-centered cubic, hexagonal, and lamellar phases were obtained by Marques and Cates.[38] The same phase diagram in "block copolymer units", i.e., replacing the temperature scale with χN and the asymmetry μ/λ by f, was obtained earlier by Leibler.[36] The gyroid phase ($Ia\bar{3}d$ symmetry) was only confirmed experimentally in 1994[39−41] and was not included as a trial structure when comparing free energies of different structures in these studies. However, it has subsequently been accounted for in Landau mean-field theory.[42,43]

Figure 3 shows results from simulations on four distinct microphase-separated structures, corresponding to the points illustrated on the phase diagram in Figure 2, which includes the four equilibrium structures observed for diblock copolymers. Simulations were carried out on a cubic $32 \times 32 \times 32$ lattice. A separate series of simulations were undertaken on a $64 \times 64 \times 64$ lattice, and the same structures were observed, indicating that finite size effects are not important for simulations on

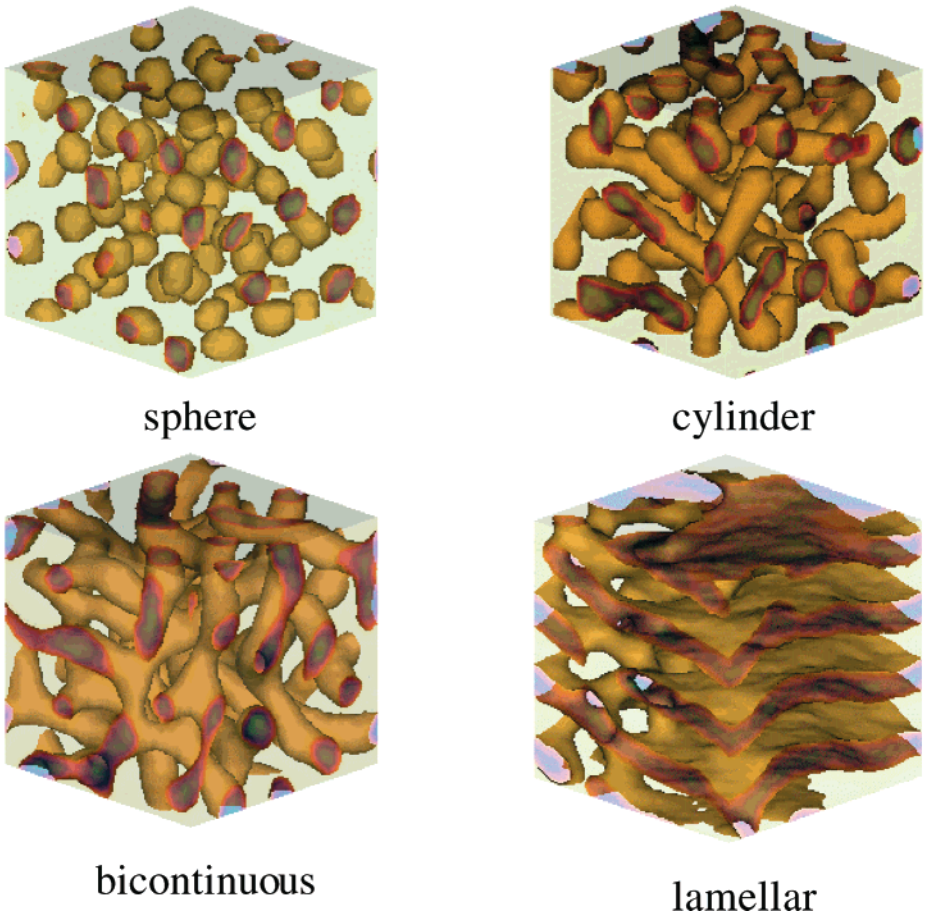

Figure 3. Examples of morphologies generated by cell dynamics simulations (starting from an initially homogeneous box). The parameters used in the simulation are listed in Table 1. Isosurfaces with $-1 < \langle\psi\rangle < -0.3$ are plotted for the sphere and cylinder structures and isosurfaces with $-1 < \langle\psi\rangle < -0.1$ for the bicontinuous and lamellar structures.

Table 1. Parameters Used in the Simulations Shown in Figure 3

	A	τ	f	u	v	D	B
spheres	1.5	0.10	0.40	0.38	2.3	0.2	0.01
cylinders	1.5	0.30	0.40	0.38	2.3	0.4	0.02
bicontinuous	1.5	0.33	0.44	0.38	2.3	0.5	0.02
lamellar	1.5	0.36	0.48	0.38	2.3	0.7	0.02

sufficiently large lattices. All the simulations were started from an initial random disordered state (ψ was a random number within the range ± 0.05) and run for up to 70 000 simulation time steps to achieve equilibrium. The parameters used in the simulation runs corresponding to Figure 3 are listed in Table 1. We term the structures "spheres", "cylinders", "bicontinuous", and "lamellar" based on the observed morphology and the calculated structure factor. It is evident that long-range lattice ordering has not developed for any phase; i.e., the spheres do not lie on a bcc lattice, the cylinders are not on a hexagonal lattice, the bicontinuous channels are not on a cubic lattice, and the lamellae are not stacked in a one-dimensional lattice. Although the channels in the bicontinuous structure have 3-fold connecting nodes, suggesting a gyroid morphology, the lack of long-range lattice order prohibits identification of this morphology based on the present simulations. The lack of long-range lattice in the four simulations order is not surprising, given the initial random starting configuration.

The structure factor, $S(q)$, obtained from simulations on $64 \times 64 \times 64$ lattices are shown in Figure 4. This shows a strong primary peak, centered at q^*, for all morphologies, corresponding to a microphase-separated structure. For the lamellar structure a strong second-order reflection is observed close to $2q^*$, as expected, confirming the tentative identification of a lamellar structure. For the bicontinuous structure, there is a broad secondary peak also close to $2q^*$. For a bicontinuous structure such as the cubic gyroid phase observed experimentally, a sequence of closely spaced higher order reflections is expected.[1] Given the small size of the simulations and the lack of long-range lattice ordering, it is not surprising that these cannot be resolved in our data. However, the morphology can be distinguished in real space from the lamellar structure, because two co-continuous labyrinths are apparent for the bicontinuous structure, with 3-fold coordinated nodes for the shaded labyrinth (Figure 3). In contrast, the lamellar structure resembles a randomly perforated membrane or "sponge". For the sphere and cylinder structures, the lack of long-range lattice ordering suggests that the broad secondary maxima in $S(q)$ should be interpreted as arising from the "form factor" of isolated spheres or cylinders. Calculations of the form factor maxima for the sphere structure (using the tabulated expression for a uniform sphere[44] show that the secondary maximum in $S(q)$ corresponds to spheres with a diameter of 6.6 lattice units, close to the diameter of 5−7 lattice units that can be measured directly from images of the morphology. Similarly, for the cylinder structure, the observed secondary peak maximum corresponds, using the form factor for an infinite uniform cylinder,[44] to a diameter of 10.5 lattice units, close to

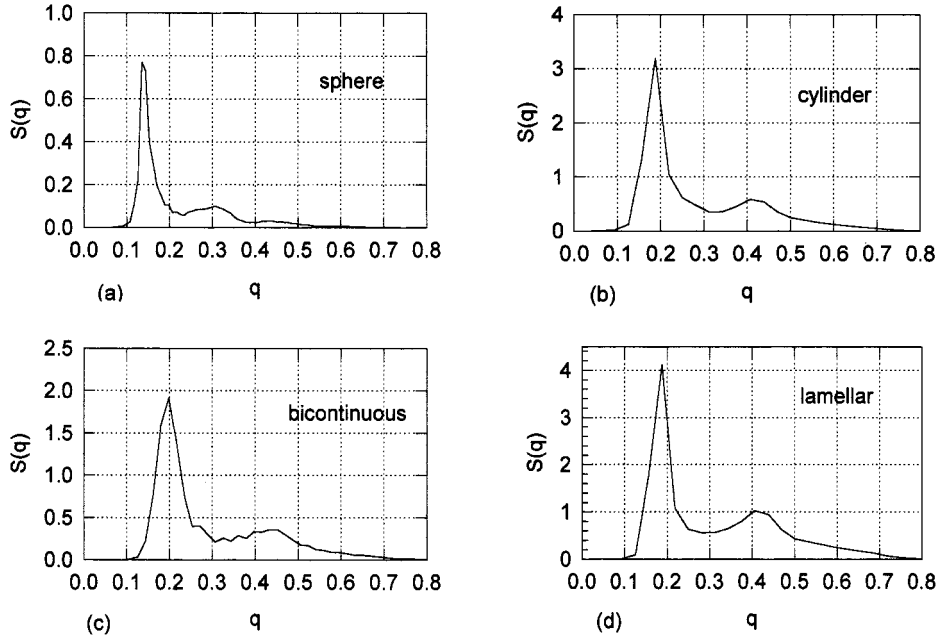

Figure 4. Structure factor obtained for the four morphologies shown in Figure 3 (results from simulations on a 64 × 64 × 64 lattice).

the 8−11 lattice units measured from the real space image.

Application of a symmetry-breaking field should lead to macroscopic alignment of mesophases so that the lattice symmetry is revealed. Preliminary work where the effect of oscillatory shear on the lamellar and cylindrical phase is simulated supports this idea because it shows orientation of lamellae and cylinders with respect to the shear direction. The structure factor from these oriented morphologies also shows the higher order Bragg reflections expected for lamellar and hexagonal microphase-separated structures. Further studies on cell dynamics simulations of shear-induced orientation will be the subject of future work.

Kinetics of Phase Separation (Effect of Phenomenological Diffusion Coefficient and Long-Range Ordering Term). The kinetics of microphase separation are controlled by the parameters in the CDS model, such as D, B, τ, and η. In the early stage of phase separation, the kinetics can be studied via a linear stability analysis, as performed for example by Qi and Wang, who computed the development of structures within a single wavenumber approximation, valid for weakly segregated morphologies.[26,27] However, to study the kinetics for all stages of the phase separation process, and also for structures of arbitrary degrees of segregation, it is necessary to undertake numerical simulations. In this study, we perform simulations to elucidate the effects and limits of D and B on the formation of microstructures and the associated ordering kinetics. In previous simulation studies,[26,27] fixed values of D and B were used.

Figure 5 shows the effect of D on the appearance of the microphase-separated structures of cylinders and lamellae. It is apparent that the cylinders become thicker in diameter and shorter in length when the value of D increases. In the lamellar phase the thickness of the layers increases as D increases, which is confirmed by Fourier transformation of projections of the structure and identification of the principal wavenumber associated with the lamellar ordering.

The mean absolute value of the order parameter $\langle|\psi(\mathbf{r},t)|\rangle$ averaged over the simulated lattice provides an indication of the extent of microphase separation in the morphology. Figure 6 shows this quantity for the cylindrical phase as a function of time (in units of simulation time steps). It can be noticed that, as D decreases, the mean absolute value of the order parameter at equilibrium increases. This is the well-known effect of D in free energies containing square gradient terms such as eq 9. The coefficient D is a surface energy term that can be considered as an effective diffusion coefficient, acting to reduce the segregation between components. In the random phase approximation it is proportional to b^2, where b is a polymer segment length.[45]

Because of the inclusion of the long-range interaction term in the free energy, eq 8, our cell dynamics simulations of block copolymers do not belong to the same universality class as the Cahn−Hilliard−Cook equation. The CHC equation exhibits dynamical scaling, where in the early stages the characteristic length grows as $L(t) \sim t^{1/3}$.[46] A similar scaling has been reported from cell dynamics simulations in the early stage of ordering of strongly segregated block copolymers.[20,47] The long-range interactions in block copolymers stop the domain coarsening at long times, as observed in our simulations. However, a general model for the ordering kinetics of block copolymers has yet to be developed, although it has been suggested that two-dimensional lamellar formation in block copolymers belongs to the same universality class as Rayleigh−Benard convection.[21,23] We have therefore adopted a phenomenological approach, using an Avrami equation to approximate the time dependence of the mean order parameter. We write an Avrami equation in the form

$$\langle|\psi(\mathbf{r},t)|\rangle = k_1 - k_2 \exp(-(t/t_c)^n) \qquad (14)$$

Here $\langle|\psi(\mathbf{r},t)|\rangle$ is the mean of the absolute value of the order parameter at time t and k_1, k_2 are constants. The Avrami exponent n reflects the nature of the phase

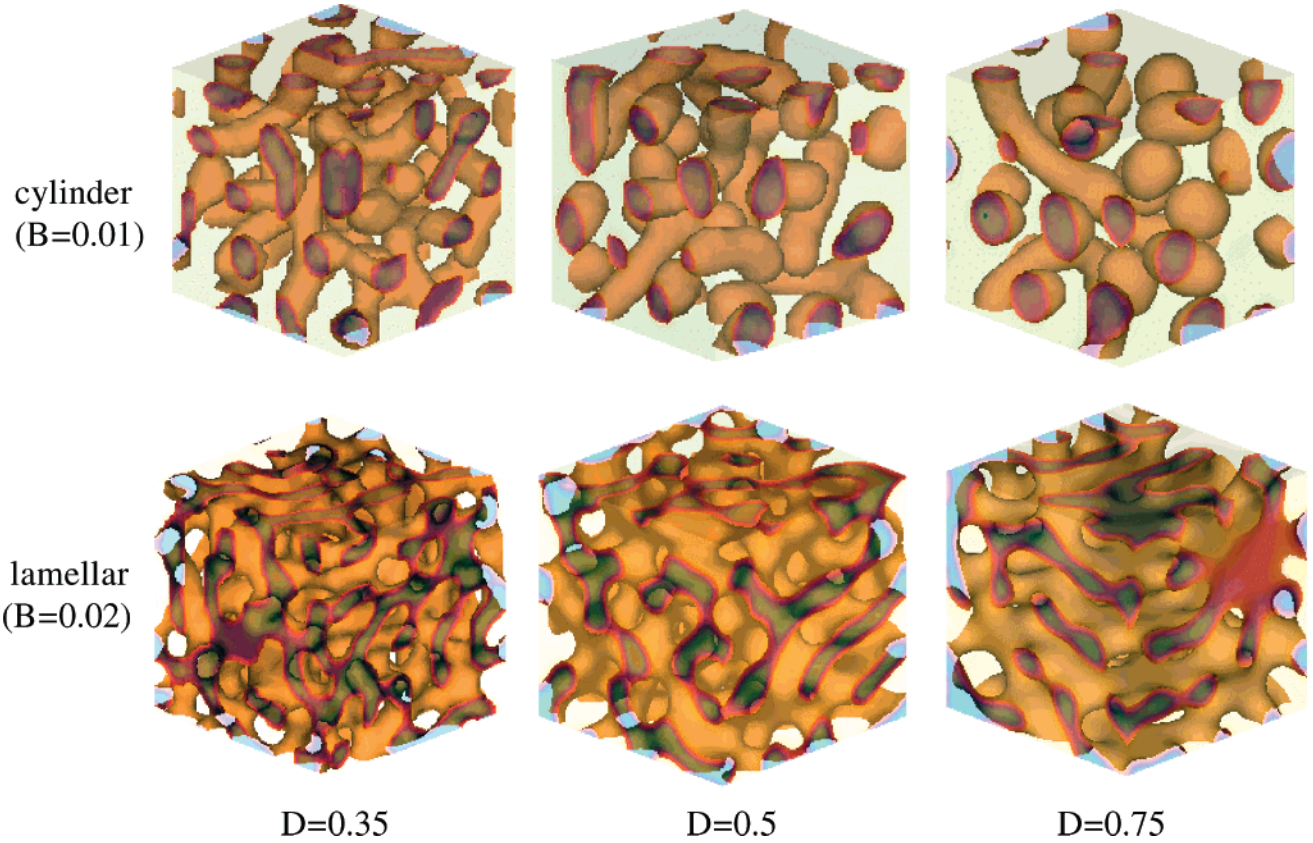

Figure 5. Effect of D on the morphology of cylinder and lamellar structures. Parameter D is a phenomenological diffusion coefficient. In the simulation, the values of A, u, and v were fixed as $A = 1.5$, $u = 0.38$, and $v = 2.3$ for both cases. For cylinders, $\tau = 0.30$, $f = 0.4$, and $B = 0.01$, while in the case of lamellae, $\tau = 0.36$, $f = 0.48$, and $B = 0.02$.

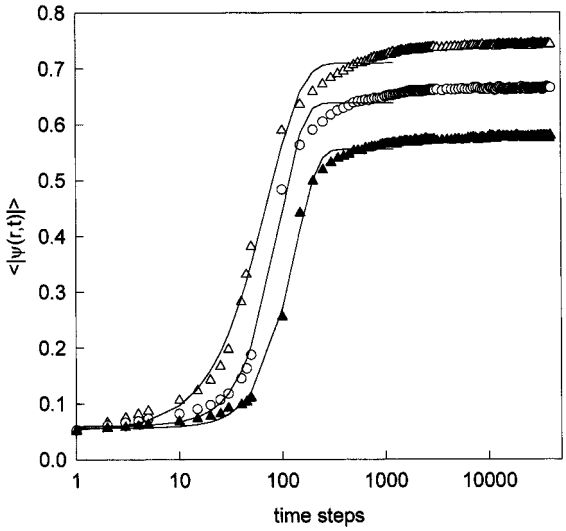

Figure 6. Kinetics of ordering from the initially disordered phase to a cylinder phase for three different values of D: (△) $D = 0.35$, (○) $D = 0.50$, and (▲) $D = 0.75$. The solid lines are fits to Avrami equations (eq 14). The fit coefficients are listed in Table 2.

separation process,[48] and t_c is the characteristic ordering time. It is emphasized that we have used Avrami equations to analyze the kinetics because it is a simple model with a minimum number of adjustable parameters that can approximately fit the data. We do not interpret the exponent n in terms of a nucleation and growth mechanism for the ordered phase because the simulation box is too small to analyze such processes. We only use the characteristic ordering time to quantify the kinetics. The values of t_c found from fits using eq 14 are listed in Table 2. This shows that the rate of development of the ordered phase increases when D decreases. This is because D reflects the tendency for diffusion against the direction of the composition gradient (i.e., for an AB diblock, A diffuses away from A-rich regions). Similar results were obtained for bicontinuous and sphere phases.

Table 2. Avrami Fit Coefficients[a]

simulation		Avrami coeffs t_c	Avrami coeffs n
cylinder phase (D effect)	$D = 0.35$	74	1.32
	0.50	96	1.92
	0.75	134	2.00
lamellar phase (τ effect)	$\tau = 0.25$	244	1.46
	0.28	162	1.84
	0.31	124	1.85
	0.35	94	1.76

[a] Parameters as defined in eq 6 and eq 13.

The top two pictures in Figure 7 show bicontinuous structures with $D = 0.35$ and $D = 0.5$, respectively, while all other parameters were fixed. Also shown in Figure 7 is the effect of B on the bicontinuous structure. It can be observed that as B increases (from 0.005 to 0.03), the diameters of the channels forming the colored network decrease. This is opposite to the effect when varying D because the scaling of D and B with polymer dimensions is opposite. In fact, B scales as b^{-2} [33] whereas $D \propto b^2$. In contrast to the effect on the size of a structure, D and B both have the same effect in regard to ordering kinetics; i.e., ordering is faster when either D or B is decreased (data for ordering kinetics as a function of B not shown). The latter arises because decreasing B leads to larger scale structures which are

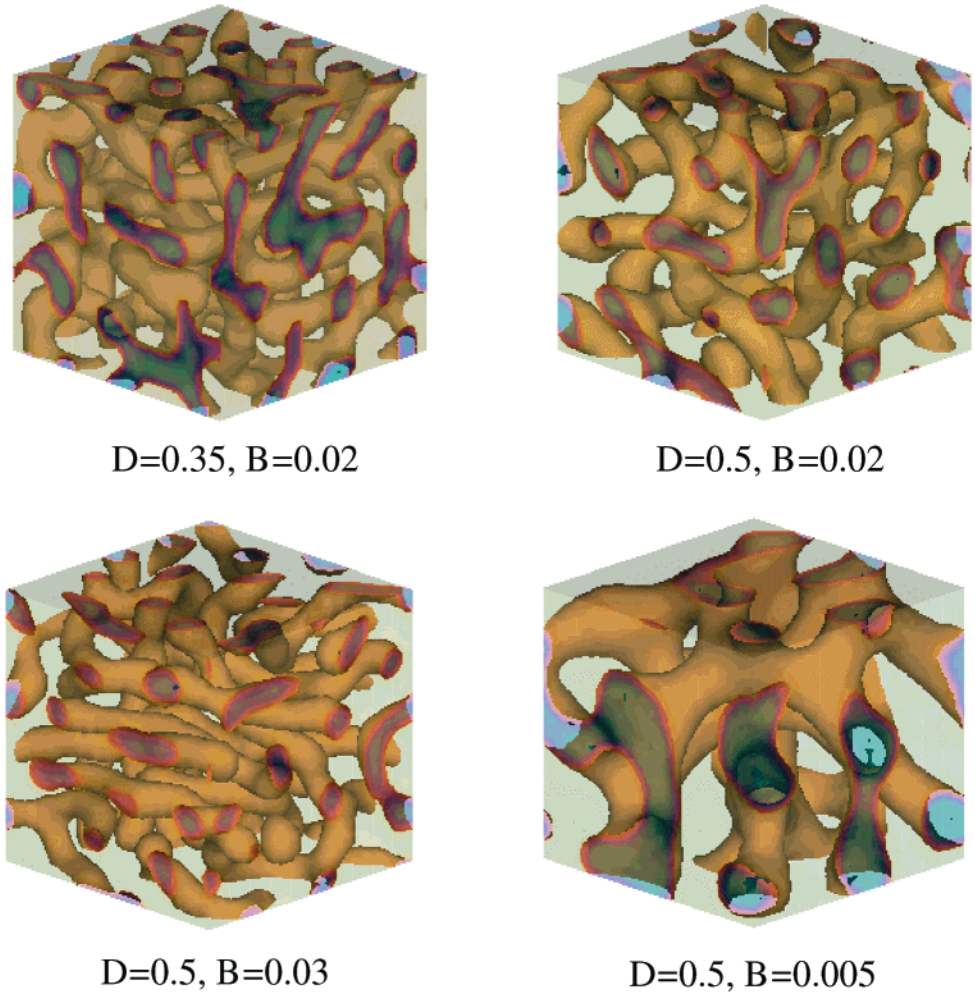

Figure 7. Effect of the magnitude of the long-range connectivity term, B, on the morphology of the bicontinuous structure. For $B = 0.02$, comparison between structures with different values of D is also made. The following parameters were fixed: $A = 1.5$, $\tau = 0.33$, $f = 0.44$, $u = 0.38$, $v = 2.3$, and $\eta = 0.05$.

formed more rapidly because the local restructuring that accompanies microphase separation is not required.

Figure 8 shows simulated structures for different values of B for the cylinder phase. For very low values of B (e.g., $B = 0.002$), large phase-separated cylinders were formed. In fact, when $B = 0$, macrophase separation was observed, as expected since this limit corresponds to the limit of ordinary spinodal decomposition.[20] On the other hand, when larger B was chosen, smaller and more spherically shaped structures (close to those observed for the spherical phase) were formed. It thus appears from our simulations on both bicontinuous and cylindrical phases that increasing B leads to a reduction in the length scale of the ordered structure. It is necessary to tune B to a value around $B \approx 0.01-0.02$ to successfully mimic experimentally observed morphologies (similar values were used to generate all patterns in Figure 3; see Table 1).

Effect of Quench Temperature. The kinetics of formation of an ordered phase are also significantly affected by the temperature-like τ parameter. Figure 9 shows the time dependence of the mean order parameter development for different values of τ. For all four cases, equilibrium was quickly reached within 1000 time steps, but $\langle|\psi(\mathbf{r},t)|\rangle$ increases as τ increases, as expected since stronger phase separation occurs for deeper quenches. The Avrami equation was used to fit the kinetic curves. The plot in the inset of Figure 9 shows the variation of the ordering time as a function of τ. It is evident that the τ parameter not only controls the equilibrium state of the phase structure but also influences the phase separation kinetics.

Effect of Thermal Noise. In the Cahn−Hilliard−Cook equation, eq 7, $\xi(r,t)$ represents a random noise of amplitude η. The noise can have an internal (thermal fluctuation) or external origin (for example, an imposed vibration). In this study, the noise field $\xi(\mathbf{r},t)$ was taken from a Gaussian random distribution[34] in the interval $[-\eta,\eta]$ for the conserved order parameter. It has been reported that there was no difference in the structure formed in cell dynamics simulations when using either a uniform or a Gaussian distributed noise term in a nonconserved system.[21]

We have observed that the effect of thermal noise is most evident in simulations in two dimensions.[49] Figure 10 shows simulated stripe structures both with and without added noise. The simulation was run on a 256 × 256 square lattice, with 90 000 time steps for equilibration. We have observed that the pattern evolution involves two stages: the rapid building of pattern amplitude followed by the slow annihilation of defects. The pattern amplitude can be characterised by $\langle|\psi(\mathbf{r},t)|\rangle$, while the defectiveness of the pattern (stripe elongation and orientation) has been characterized using an orientation correlation parameter.[49] The patterns shown in Figure 10 clearly demonstrate that increasing ther-

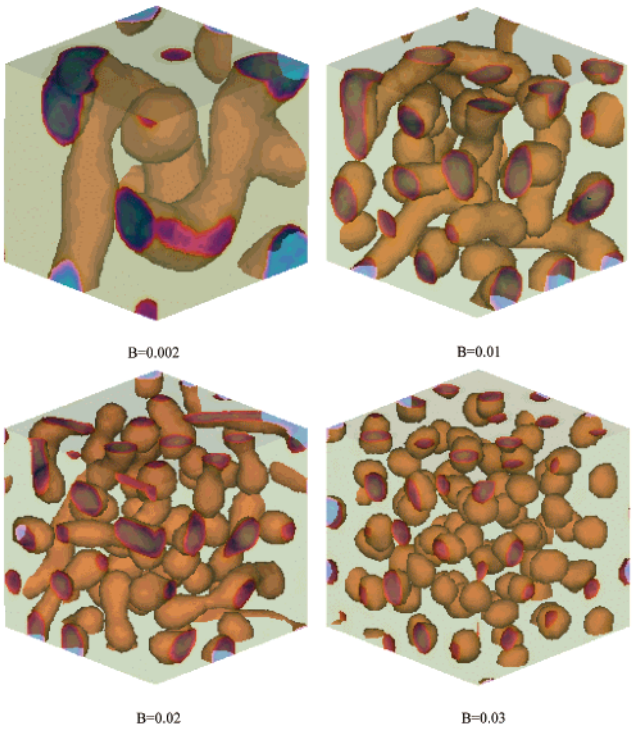

Figure 8. Effect of B on the morphology of the cylinder structure. $B = 0$ corresponds to macrophase separation, whereas a value of $B = 0.03$ leads to a structure where the cylinders are pinched off into nearly spherical aggregates. The following parameters were fixed: $A = 1.5$, $\tau = 0.31$, $f = 0.41$, $u = 0.30$, $v = 2.3$, $D = 0.5$, and $\eta = 0.1$.

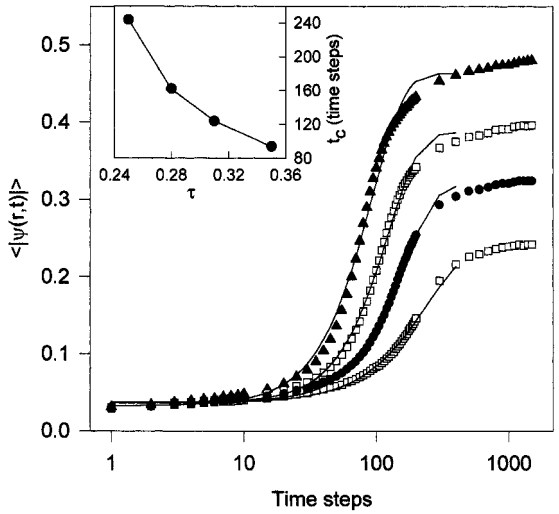

Figure 9. Effect of quench depth (final temperature τ) on the ordering kinetics of a lamellar structure from an initial disordered phase: (□) $\tau = 0.25$, (●) $\tau = 0.28$, (○) $\tau = 0.31$, and (▲) $\tau = 0.35$. The solid lines are fits to the Avrami equation (eq 14). The fit coefficients are listed in Table 2. Inset: characteristic ordering times, t_c (obtained from the Avrami model fits), as a function of temperature τ. In the simulation, we chose $A = 1.5$, $f = 0.49$, $u = 0.38$, $v = 2.3$, $\eta = 0.05$, $D = 0.5$, and $B = 0.02$.

mal noise leads to local annealing of defects and elongation of the stripes. The value of $\langle|\psi(\mathbf{r},t)|\rangle$ reached equilibrium before 2000 time steps in both cases. The pattern was then frozen in the case of zero noise, while the defect annihilation process continued up to 90 000 time times in the case of $\eta = 0.1$. It is clear that the noise term enhances the pattern orientation and stripe elongation in 2D systems.

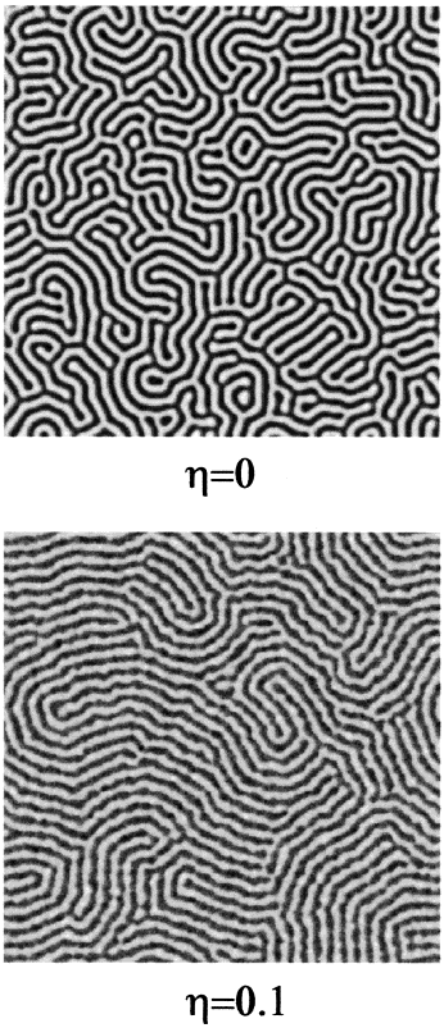

Figure 10. Effect of the amplitude of thermal noise ($\eta = 0$ and 0.1, respectively) on the orientation of a two-dimensional stripe pattern.[49] Increasing thermal noise leads to an annealing effect, producing stripes with enhanced local orientational correlations. The simulation parameters were as follows: $A = 1.5$ $\tau = 0.35$, $f = 0.5$, $u = 0.5$, $v = 1.5$, $D = 0.5$, and $B = 0.02$.

The noise effect on 3D systems is complicated and not as easy to visualize and characterize as for 2D systems. Figure 11 enables a comparison of structures developed for sphere, cylinder, bicontinuous, and lamellar phases in the cases with noise and without noise. The other parameters were fixed for each phase in the simulation, and the simulation was run up to 40 000 time steps in each case. The noise appeared to be crucial for development of the spherical phase. We believe that this is because the free energy minimum in the absence of noise is too shallow. Numerical modeling of the kinetics of phase separation in binary mixtures via the CHC equation also indicates that an initial large random perturbation is required to nucleate phase separation for off-critical quenches, where the homogeneous phase is not as unstable as for critical quenches.[50] Our simulations for the sphere phase revealed that without noise ($\eta = 0$) there is no phase separation (the system evolved to total disorder ($\psi = 0$) after several hundred time steps, from an initial random state with η defined in the range [−0.025,0.025]). Microphase separation was only observed when noise was added above a threshold

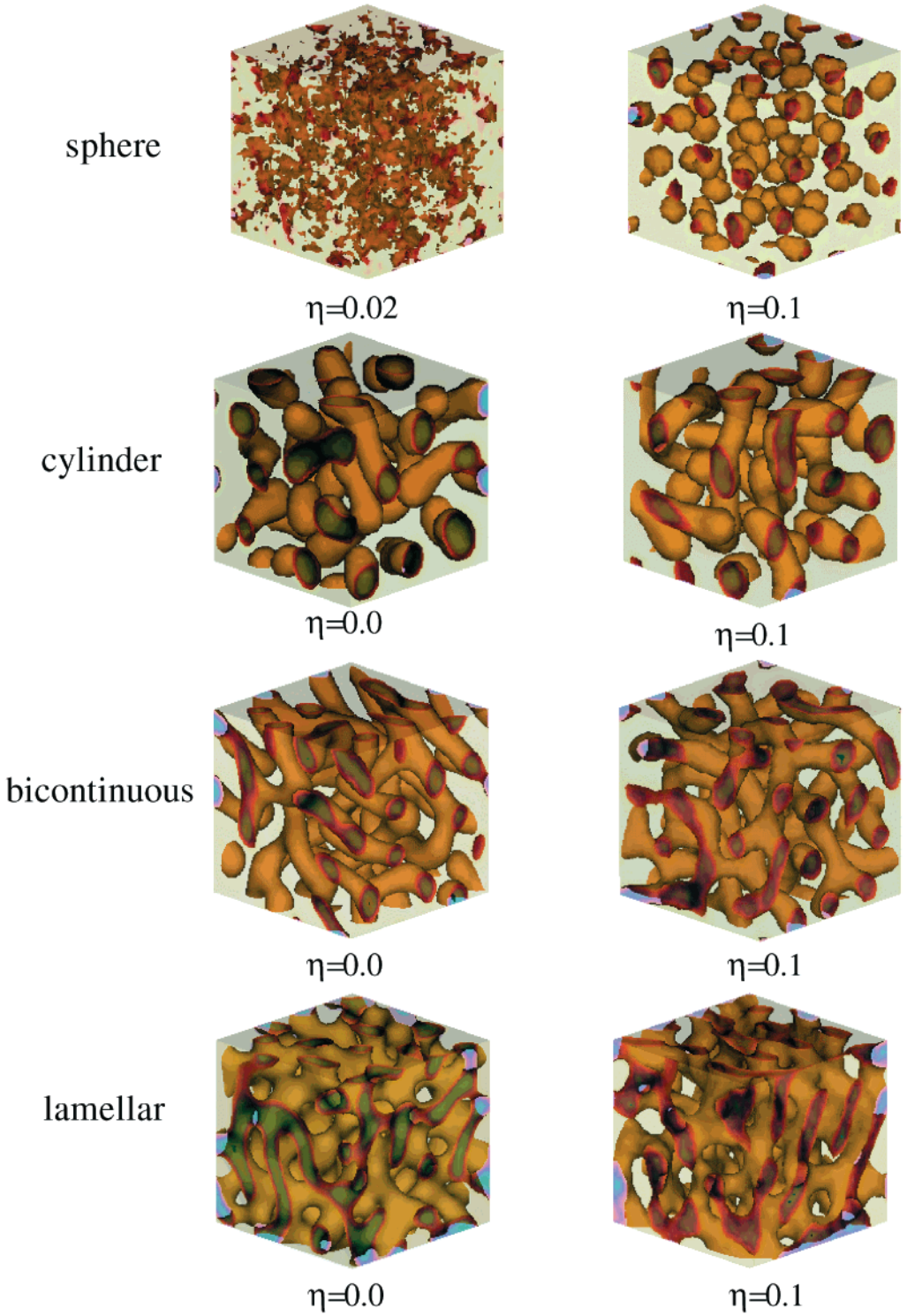

Figure 11. Effect of thermal noise on the morphology of block copolymer mesophases in three dimensions. Thermal noise is essential to generate well-defined spheres, which occurs at high temperatures in the phase diagram (Figure 2). However, the other morphologies can be generated with $\eta = 0$.

level. Regular spherical domains only appeared for $\eta >$ 0.03 in the case simulated. For the cylinder phase, it can be seen that the cylinders become somewhat elongated when the noise level is increased to $\eta = 0.1$. In the cases of bicontinuous and lamellar phases, it is difficult to quantify any significant changes of the pattern when comparing simulations performed with and without noise.

Figure 12 shows the evolution of the mean value of the order parameter for the development of the sphere phase for three different noise levels. The curves have been fitted using Avrami equations. The results show that the same equilibrium pattern amplitude, $\langle|\psi(\mathbf{r},t)|\rangle$, is reached when a well-defined spherical morphology forms, while the ordering time was reduced when the noise level was increased from $\eta = 0.05$ to $\eta = 0.1$. This is the same trend observed for the 2D systems. Similar results have been obtained for cylinder, bicontinuous, and lamellar phases. In general, the added noise reduces the ordering time and may elongate and orient the

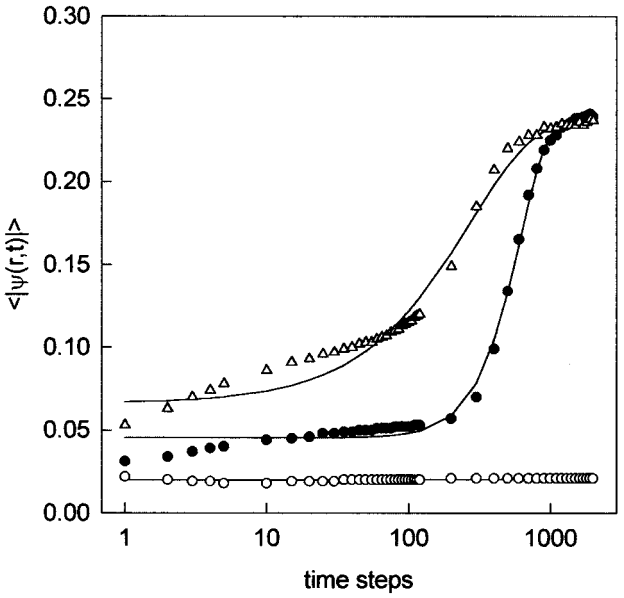

Figure 12. Effect of thermal noise on the ordering kinetics of a spherical phase. The simulation parameters were as follows: $A = 1.5$, $\tau = 0.10$, $f = 0.4$, $u = 0.38$, $v = 2.3$, $D = 0.2$, $B = 0.01$. (○) $\eta = 0.02$, (●) $\eta = 0.05$, and (△) $\eta = 0.1$.

patterns in 3D systems as in 2D, but it has no effect on the equilibrium pattern amplitude. As yet it has not proved possible to quantify the orientation changes in the 3D structures in a straightforward manner.

Conclusions

We have shown that cell dynamics simulations are an effective tool to generate randomly oriented microphase structures consistent with a Landau mean-field theory for diblock copolymers. Starting from an initial disordered state, sphere, cylinder, bicontinuous, and lamellar morphologies can be generated by appropriate selection of ordering temperature and copolymer asymmetry. It is also necessary to tune the effective diffusion coefficient and magnitude of the long-range ordering term to generate morphologies resembling those observed experimentally. In the case of the highest temperature ordered phase, the sphere phase, we have found it necessary to add finite thermal noise term to generate microphase-separated spheres. This is believed to be due to the important role of composition fluctuations at high temperature, which are simulated by addition of thermal noise.

The effects of the effective diffusion coefficient, D, and the magnitude of the long-range contribution to the free energy, B, have been explored in detail. Increasing D leads, as expected, to a lower degree of segregation between larger microdomains. In addition, microphase-separated structures are smaller. In contrast, increasing B leads to smaller minority domains. This is because B scales as b^{-2} whereas $D \propto b^2$.

The kinetics of ordering from the disordered phase have been investigated as a function of all simulation parameters. The increase in the system-averaged absolute order parameter is approximated by Avrami equations with variable rate coefficients and exponents. For a given morphology, the ordering is faster when D or B is decreased, when thermal quench depth is increased or when the amplitude of thermal noise is increased.

In future work, it will be interesting to extend the method to more complex systems such as ABC triblock copolymers, where there are two independent composition fields. This will require generalization of the cell dynamics scheme to the case of two order parameters. This is of particular interest, since a phase diagram for such systems in mean-field theory is lacking due to the large number of possible "trial structures", the free energy of which would need to be compared to predict equilibrium ordered phases. Cell dynamics simulations could complement other recently developed[51,52] methods of exploring equilibrium morphospace that do not require a priori assumptions about the symmetry of the ordered structure.

Acknowledgment. S.R.R. was supported by the Engineering and Physical Sciences Research Council, UK (grant reference GR/M08523). We thank Paulo Teixeira for stimulating discussions.

References and Notes

(1) Hamley, I. W. *The Physics of Block Copolymers*; Oxford University Press: Oxford, 1998.
(2) Matsen, M. W.; Schick, M. *Phys. Rev. Lett.* **1994**, *72*, 2660.
(3) Matsen, M. W.; Bates, F. S. *Macromolecules* **1996**, *29*, 7641.
(4) Matsen, M. W.; Bates, F. S. *Macromolecules* **1996**, *29*, 1091.
(5) Oono, Y.; Puri, S. *Phys. Rev. Lett.* **1987**, *58*, 836.
(6) Oono, Y.; Puri, S. *Phys. Rev. A* **1988**, *38*, 434.
(7) Puri, S.; Oono, Y. *Phys. Rev. A* **1988**, *38*, 1542.
(8) Shinozaki, A.; Oono, Y. *Phys. Rev. Lett.* **1991**, *66*, 173.
(9) Shinozaki, A.; Oono, Y. *Phys. Rev. A* **1992**, *45*, 2161.
(10) Shinozaki, A.; Oono, Y. *Phys. Rev. E* **1993**, *48*, 2622.
(11) Ohta, T.; Nozaki, H.; Doi, M. *J. Chem. Phys.* **1990**, *93*, 2664.
(12) Ohta, T.; Nozaki, H.; Doi, M. *Phys. Lett. A* **1990**, *145*, 304.
(13) Kodama, H.; Doi, M. *Macromolecules* **1996**, *29*, 2652.
(14) Komura, S.; Kodama, H. *Phys. Rev. E* **1997**, *55*, 1722.
(15) Roan, J.-R.; Shaknovich, E. I. *Phys. Rev. E* **1999**, *59*, 2109.
(16) Ginzburg, V. V.; Qui, F.; Paniconi, M.; Peng, G.; Jasnow, D.; Balazs, A. C. *Phys. Rev. Lett.* **1999**, *82*, 4026.
(17) Oono, Y. *Int. J. Mod. Phys. B* **1993**, *7*, 1859.
(18) Teixeira, P. I. C.; Mulder, B. M. *Phys. Rev. E* **1996**, *53*, 1805.
(19) Massunaga, M. S. O.; Paniconi, M.; Oono, Y. *Phys. Rev. E* **1997**, *56*, 723.
(20) Bahiana, M.; Oono, Y. *Phys. Rev. A* **1990**, *41*, 6763.
(21) Taneike, T.; Shiwa, Y. *J. Phys.: Condens. Matter* **1997**, *9*, L147.
(22) Komura, S.; Fukuda, J.-I.; Paquette, G. C. *Phys. Rev. E* **1996**, *53*, 5588.
(23) Shiwa, Y.; Taneike, T.; Yokojima, Y. *Phys. Rev. Lett.* **1996**, *77*, 4378.
(24) Ohta, T.; Enomoto, Y.; Harden, J. L.; Doi, M. *Macromolecules* **1993**, *26*, 4928.
(25) Zhang, H.; Zhang, J.; Yang, Y.; Zhou, X. *J. Chem. Phys.* **1997**, *106*, 784.
(26) Qi, S.; Wang, Z. G. *Phys. Rev. Lett.* **1996**, *76*, 1679.
(27) Qi, S.; Wang, Z. G. *Phys. Rev. E* **1997**, *55*, 1682.
(28) Hamley, I. W.; Ren, S. R. *Macromol. Theory Simul.* **2000**, *9*, 363.
(29) Zvelindovsky, A. V.; Sevink, G. J. A.; van Vlimmeren, B. A. C.; Maurits, N. M.; Fraaije, J. G. E. M. *Phys. Rev. E* **1998**, *57*, 4879.
(30) Sevink, G. J. A.; Zvelindovsky, A. V.; van Vlimmeren, B. A. C.; Maurits, N. M.; Fraaije, J. G. E. M. *J. Chem. Phys.* **1999**, *110*, 2250.
(31) van Vlimmeren, B. A. C.; Maurits, N. M.; Zvelinodvsky, A. V.; Sevink, G. J. A.; Fraaije, J. G. E. M. *Macromolecules* **1999**, *32*, 646.
(32) Maurits, N. M. PhD Thesis, University of Groningen, 1998.
(33) Ohta, T.; Kawasaki, K. *Macromolecules* **1986**, *19*, 2621.
(34) The noise satisfies the fluctuation−dissipation theorem. To ensure approximate conservation of the order parameter, we have adapted to the 3D case the procedure described for 2D systems in: Ball, R. C.; Essery, R. L. H. *J. Phys.: Condens. Matter* **1990**, *2*, 10303. Specifically, three independent Gaussian distributed random numbers $\xi_l(i,j,k)$, $\xi_m(i,j,k)$, and $\xi_n(i,j,k)$ are generated at each lattice point (i,j,k), representing fluctuations in different directions. The noise term is then taken as $\eta\xi(r,t) = \eta[\xi_l(i,j,k) - \xi_l(i\pm1,j,k) + \xi_m(i,j,k) - \xi_m(i,j\pm1,k) + \xi_n(i,j,k) - \xi_n(i,j,k\pm1)]$ at each time step. A third set of uniformly distributed random numbers is used to

determine whether "±" takes "+" or "−" in the calculation. The amplitude of the noise level is denoted η.
(35) Teixeira, P. I. C.; Mulder, B. M. *Phys. Rev. E* **1997**, *55*, 3789.
(36) Leibler, L. *Macromolecules* **1980**, *13*, 1602.
(37) Semenov, A. N. *Sov. Phys. JETP* **1985**, *61*, 733.
(38) Marques, C. M.; Cates, M. E. *Europhys. Lett.* **1990**, *13*, 267.
(39) Schulz, M. F.; Bates, F. S.; Almdal, K.; Mortensen, K. *Phys. Rev. Lett.* **1994**, *73*, 86.
(40) Hajduk, D. A.; Harper, P. E.; Gruner, S. M.; Honeker, C. C.; Kim, G.; Thomas, E. L.; Fetters, L. J. *Macromolecules* **1994**, *27*, 4063.
(41) Förster, S.; Khandpur, A. K.; Zhao, J.; Bates, F. S.; Hamley, I. W.; Ryan, A. J.; Bras, W. *Macromolecules* **1994**, *27*, 6922.
(42) Podneks, V. E.; Hamley, I. W. *JETP Lett.* **1996**, *64*, 617.
(43) Hamley, I. W.; Podneks, V. E. *Macromolecules* **1997**, *30*, 3701.
(44) Kerker, M. *The Scattering of Light*; Academic Press: New York, 1969; pp 482−483.
(45) Jones, R. A. L.; Richards, R. W. *Polymers at Surfaces and Interfaces*; Cambridge University Press: Cambridge, 1999.
(46) Lifshitz, I. M.; Slyozov, V. V. *J. Phys. Chem. Solids* **1961**, *19*, 35.
(47) Oono, Y.; Bahiana, M. *Phys. Rev. Lett.* **1988**, *61*, 1109.
(48) Gedde, U. W. *Polymer Physics*; Chapman and Hall: London, 1995.
(49) Ren, S. R.; Hamley, I. W.; Teixeira, P. I. C.; Olmsted, P. D. *Phys. Rev. E*, in press.
(50) Chakrabarti, A.; Toral, R.; Gunton, J. D. *Phys. Rev. E* **1993**, *47*, 3025.
(51) Drolet, F.; Fredrickson, G. H. *Phys. Rev. Lett.* **1999**, *83*, 4317.
(52) Bohbot-Raviv, Y.; Wang, Z. G. *Phys. Rev. Lett.* **2000**, *85*, 3428.

MA000678Z